**Title:** Hallmarks of frailty and osteosarcopenia in prematurely aged PolgA$^{D257A/D257A}$ mice: a preclinical model to test anabolic interventions

**Authors:** Ariane C. Scheuren[1†], Gommaar D'Hulst[2†], Gisela A. Kuhn[1], Evi Masschelein[2], Esther Wehrle[1], Katrien De Bock[2], Ralph Müller[1*]

**Affiliations:**

[1] Institute for Biomechanics, ETH Zurich, Zurich, Switzerland.

[2] Laboratory of Exercise and Health, ETH Zurich, Zurich, Switzerland.

†Co-first authors

*Corresponding author:

Prof. Ralph Müller, PhD

Institute for Biomechanics, ETH Zurich, Zurich, Switzerland

Leopold-Ruzicka-Weg 4, 8093, Zurich, Switzerland

ram@ethz.ch

**Keywords:** aging, frailty, osteopenia, sarcopenia, osteosarcopenia, mouse, mTORC1, in vivo micro-CT

**One Sentence Summary:** PolgA mice exhibit hallmarks of human frailty and osteosarcopenia, allowing identification of underlying mechanisms and potential interventions.


## Abstract

Frailty is a geriatric syndrome characterized by increased susceptibility to adverse health outcomes. One major determinant thereof is the gradual weakening of the musculoskeletal system and the associated osteosarcopenia. To improve our understanding of the underlying pathophysiology and, more importantly, to test potential interventions aimed at counteracting frailty suitable animal models are needed. Here, we report the relevance of a mouse model of accelerated aging (PolgA$^{(D257A/D257A)}$) as a model for frailty and osteosarcopenia. The longitudinal assessment of the clinical mouse frailty index showed that PolgA$^{(D257A/D257A)}$ mice accumulated health deficits at a higher rate compared to wild type littermates (PolgA$^{(+/+)}$, WT). Concomitantly, PolgA$^{(D257A/D257A)}$ mice displayed progressive musculoskeletal deterioration such as reduced bone and muscle mass as well as impaired functionality thereof. Specifically, PolgA$^{(D257A/D257A)}$ had lower grip-strength and concentric muscle forces as well as reduced bone turnover as assessed by longitudinal micro-CT. In addition, PolgA$^{(D257A/D257A)}$ mutation altered the sensitivity to anabolic stimuli in skeletal muscle, muscle progenitors and bone. While, compared to WT, PolgA$^{(D257A/D257A)}$ caudal vertebrae were not responsive to a cyclic loading regime, PolgA$^{(D257A/D257A)}$ muscles were hypersensitive to eccentric contractions as well as leucine administration, shown by larger downstream signaling response of the mechanistic target of rapamycin complex 1 (mTORC1). However, myogenic progenitors cultured *in vitro* showed severe anabolic resistance to leucine and robust impairments in cell proliferation. Overall, PolgA$^{(D257A/D257A)}$ mutation leads to hallmarks of age-related frailty and osteosarcopenia as observed in humans and thus, provides a powerful model to better understand the relationship between frailty and the aging musculoskeletal system.

## Introduction

Although there is no universally accepted definition of frailty (*1*), it is considered as an age-related syndrome characterized by the decline of multiple physiological functions, leading to the accumulation of health deficits, and thus a higher vulnerability to adverse health outcomes such as morbidity and mortality (*2*). One of the most prominent components of frailty is the progressive weakening of the musculoskeletal system (*3-5*), leading to common age-related diseases such as osteopenia and sarcopenia. There is growing evidence that both diseases often co-exist in frail older individuals (also termed osteosarcopenia (*6, 7*)), thereby further increasing the risk for negative outcomes such as falls and fractures (*8, 9*). Although several anabolic interventions such as dietary protein supplementation and mechanical stimulation are known to promote muscle and bone formation in young individuals, the molecular insights behind osteopenia and sarcopenia in the elderly population are lacking. In the field of muscle physiology, studies in humans and rodents have shown that aged muscles are less responsive to well-known anabolic stimuli such as amino acids (*10-12*) and muscle contractions (*13*); this likely results from reduced protein synthesis due to diminished intracellular signaling through the mechanistic target of rapamycin complex 1 (mTORC1) pathway (*14-16*). Although this phenomenon, termed "anabolic resistance", is well described in response to single bouts of exercise or protein meals (*10-12, 17*), it appears to be dose-dependent, as the response to larger doses of protein is not reduced by age (*18, 19*). Moreover, the diminished protein synthesis response in aging adults can be rescued by combining multiple stimuli (i.e. exercise and protein meals) (*20*). Next to impairments in intra-muscular mTORC1 signaling, age-related sarcopenia has been associated with a decrease in number (*21, 22*) and proliferation capacity (*23, 24*) of myogenic progenitors or satellite cells. These are not only instrumental for the maintenance of muscle fibers, but also for the adaptive responses to exercise and regeneration upon injury (*25*). In the field of bone physiology, evidence pointing towards altered mechanosensitivity with age

has also been shown in humans (*26*) and in mice (*27-30*). However, this effect might be site-specific as studies using a tibia-loading model showed a reduced response of trabecular (*27, 28*) and cortical (*29, 30*) bone formation with age, while bone adaptation in response to loading of the caudal vertebrae was maintained with age (*31*). Therefore, whether and how age-related changes in the responsiveness to anabolic stimuli occur remains unclear. A better understanding of the pathophysiology of osteosarcopenia will help to identify interventions to strengthen the musculoskeletal system, which ultimately will be beneficial for the prevention and/or treatment of frailty.

In order to address this, tools such as the frailty index (FI) have been established to quantify the accumulation of age-related health deficits (e.g., loss of hearing, tremoring, comorbid diseases) in humans (*32*) and more recently, also in mice (*33*). Indeed, the striking similarities between key features of the FI scores in humans and in mice (*34*) have highlighted the potential of rodent frailty models to not only improve our understanding of frailty but also serve as a tool to test responses to interventions designed to modify (or even prevent) frailty (*35-37*). In this study, we therefore aimed to evaluate the PolgA$^{(D257A/D257A)}$ mouse (referred to as PolgA), which due to elevated mitochondrial DNA point mutations and systemic mitochondrial dysfunction, exhibits an accelerated aging phenotype (*38, 39*), as a model of frailty and osteosarcopenia. While these mice are known to develop multiple signs of aging (e.g., hair loss, greying, hearing loss) earlier (around 40 weeks of age) than their wild type littermates (PolgA$^{+/+}$, referred to as WT), the frailty phenotype has to the best of our knowledge not yet been assessed in these mice. Furthermore, although several studies have reported lower muscle weights in PolgA mice compared to their WT littermates (*38, 40, 41*), little is known about their muscle quality and functionality. To address this, forelimb grip-strength and concentric muscle forces were measured *in vivo* and *ex vivo*, respectively, in addition to the evaluation of hind limb muscles masses. With respect to the bone phenotype, only two studies have reported reduced femoral

bone density using X-ray densitometry (*38, 39*). Although this technique is still the gold-standard to assess bone mineral density (i.e. bone quantity) clinically in humans, it does not provide insight regarding the quality of bone tissue. Therefore, bone phenotyping in pre-clinical studies is commonly performed using high-resolution micro-computed tomography (micro-CT) as it allows additional standardized evaluation of the three-dimensional bone microarchitecture (*42*). Furthermore, using *in vivo* micro-CT, dynamic bone remodeling activities can be tracked longitudinally providing information both on bone formation and bone resorption (*29, 43*). These markers are important for better understanding of the changes in bone microarchitecture due to osteopenia. Coupled with longitudinal measurements of FI, we aimed to monitor individual mice during the process of aging, allowing us to capture the onset of osteosarcopenia and to track other signs of aging. Lastly, using a combination of established *in vivo*, *ex vivo*, and *in vitro* models, we investigated the effects of well-known anabolic stimuli (i.e. eccentric contractions, leucine administration, and mechanical loading) on the musculoskeletal system of aged PolgA mice.

## Results

### *With age, PolgA mice become frailer and display signs of co-existing osteopenia and sarcopenia*

To characterize the frailty and the musculoskeletal phenotypes of the PolgA model, female PolgA$^{(D257A/D257A)}$ (referred to as PolgA) and wild type littermates (PolgA$^{(+/+)}$, referred to as WT) were aged in parallel and sacrificed at 34, 40 and 46 weeks, respectively. Using the clinical mouse frailty index (FI) as a tool to quantify the accumulation of health deficits (*33*), we observed that older (40 and 46 weeks), but not younger (34 weeks) PolgA mice had higher FI scores compared to WT (Fig. 1A). This divergence between genotypes at later time-points was also observed when FI was assessed longitudinally in individual mice at 34, 38 and 40 weeks, respectively. Specifically, between 34 and 40 weeks, the mean FI in PolgA mice increased from

0.05±0.02 to 0.15±0.02 (mean±SD, $p<0.0001$), whereas the increase in WT from 0.04±0.03 to 0.06±0.04 was less pronounced ($p<0.05$, Fig. 1B). Thus, compared to WT, PolgA mice had 73% ($p<0.05$) and 128% ($p<0.001$) higher FI at 38 and 40 weeks, respectively. Furthermore, the slope of the natural logarithm of the FI versus age curve, which has been shown to correspond to the rate of deficit accumulation in humans (*44*), was 0.025 in PolgA mice and 0.012 in WT, suggesting that PolgA mice became frailer faster than WT ($p<0.05$, Fig. 1C).

Concomitant to the increase in FI with age, older PolgA mice displayed deteriorations of the musculoskeletal system. Specifically, the assessment of bone morphometric parameters by micro-CT showed that the apparent volume density (AVD) of PolgA femora was already 5% lower at 34 weeks of age ($p<0.05$), which became more pronounced at 40 and 46 weeks, respectively ($p<0.0001$, Fig. 1D). The total cross-sectional area of the periosteal envelope (Tt.Ar) was similar between genotypes at 34 weeks ($p>0.05$), but then diverged over time such that PolgA had lower Tt.Ar at 40 and 46 weeks ($p<0.0001$), respectively (Fig. 1E, F). Likewise, the weights of *m. extensor digitorum longus* (EDL) and fiber cross-sectional area of *m. tibialis anterior* (TA) were similar between genotypes at 34 weeks ($p>0.05$), but 20% and 22% lower in PolgA mice at 40 and 46 weeks, respectively ($p<0.05$, Fig. 1G-I). Similarly, lower weights of TA and *m. gastrocnemius* (GAS) in PolgA mice as compared to WT were observed at 40 (-20%, $p<0.0001$ and -23%, $p<0.0001$) and 46 weeks (-22%, $p<0.0001$ and -16%, $p<0.05$), respectively.

*Decreased forelimb grip-strength and concentric force in PolgA mice*

Considering that PolgA mice showed clear reductions in muscle mass and cross-sectional area at 40 and 46 weeks, we aimed to comprehensively characterize the muscular functionality at these time-points. At 40 weeks, *in vivo* assessment of the forelimb grip-strength, a widely used method to assess muscle function in rodents, showed that PolgA mice had lower grip-strength relative to bodyweight ($p<0.05$, Fig. 2A). Furthermore, when the EDL was subjected to a force-

frequency protocol, PolgA showed a tendency towards decreased absolute force at 250 and 300Hz ($p<0.10$), while relative force was not affected (Fig. 2B,C). At 46 weeks, the grip-strength was 11% lower in PolgA mice compared to WT, but did not reach significance (Fig. 2D). The differences in forces however, were more exacerbated with a lower absolute and relative force at 80 to 300Hz (absolute) and 250 to 300Hz (relative) in the PolgA ($p<0.05$, Fig. 2E,F).

*PolgA mutation induces higher basal and eccentric contraction (ECC) evoked mTORC1 and mechanotransduction signaling*

Because PolgA muscles were atrophied and weaker than those of their WT littermates of the same chronological age, we sought to verify anabolic resistance upon ECC in an isolated *ex vivo* model. ECC have been shown to effectively activate mTORC1, the main regulator of skeletal muscle protein synthesis (*45, 46*). Data of muscle forces evoked by ECC are presented in table 1. PolgA had similar average force during the 60 ECC contractions, but tended to have a lower peak force during the first set (table 1).

At 40 weeks, ECC evoked increased phosphorylation of the downstream mTORC1 kinase Ribosomal protein S6 Kinase 1(S6K1) at Thr389 compared to the contralateral control leg in both WT (+147±50%, $p<0.05$) and PolgA (406±161%, $p<0.05$), but the increase was more pronounced in PolgA resulting in a higher pS6K1 upon ECC in the PolgA ($\Delta_{ECC\text{-}CTL}$, $p<0.05$) (Fig. 3A). The direct downstream kinase of pS6K1, S6 Ribosomal Protein (RPS6) showed similar increases in phosphorylation at Ser235/236 upon ECC in WT and PolgA (64±24% and 352±146%, $p<0.05$), whereas there was only a trend towards higher activation in PolgA compared to WT ($\Delta_{ECC\text{-}CTL}$, $p=0.07$) (Fig. 3B). At 46 weeks, downstream mTORC1 targets showed similar effects with a trend towards hyper-phosphorylated pS6K1 and pRPS6 after ECC contractions in the PolgA compared to WT ($p=0.10$, Fig. 3D,E). Moreover, basal pRPS6 was

higher in PolgA (1257±427%, $p<0.05$) compared to WT (Fig. 3E), suggesting both basal and contraction-induced hyper activation of mTORC1 in PolgA mutated muscle.

One of the proposed pathways for high-load contractions to regulate mTORC1 is via activation of the stress responsive mitogen-activated protein kinase (MAPK) pathway (*47*). To investigate whether the hyperactive mTORC1 signaling in the PolgA muscle was related to increased MAPK response, we measured activation of (Stress-Activated Protein Kinase/Jun-amino-terminal Kinase) pSAPK/JNK upon ECC. At 40 weeks, the stress-responsive pSAPK/JNK at Thr138/Tyr185 after ECC increased by 113±35.8% ($p<0.05$) in WT and by 156±26% ($p<0.001$) in PolgA (Fig. 3G), with a tendency towards hyperactivation in PolgA compared to WT ($\Delta_{ECC-CTL}$, $p=0.09$). At 46 weeks, the increase in pSAPK/JNK upon ECC was more pronounced in the PolgA (2410±1035%, $p<0.05$) than in the WT (1410±179%, $p<0.05$) resulting in a higher phosphorylation in PolgA muscle after ECC ($\Delta_{ECC-CTL}$, $p<0.05$) and a tendency towards higher basal pSAPK/JNK ($p=0.07$, Fig. 3J). Interestingly, another arm of the stress-responsive MAPK pathway, p42-44 MAPK at Thr202/Tyr204, was not affected by ECC; however, basal p44/42 signaling was higher in PolgA muscle compared to WT at 46 weeks (Fig. 3H,K). These data show that hyperactive mTORC1 signaling mirrors increased basal and contraction-induced MAPK signaling in PolgA mutated muscle.

*PolgA whole muscles are hypersensitive to leucine in vivo, while their primary myotubes are resistant to leucine in vitro*

To examine whether other anabolic stimuli also hyper activate mTORC1 signaling in PolgA muscle, we administered a submaximal (0.4g/kg) dose of leucine via gavage to 46-week-old WT and PolgA littermates. Leucine induced an increase in pRPS6 in both WT ($p<0.05$) and PolgA ($p<0.0001$) TA, whereas pS6K1 was also increased in PolgA ($p<0.001$). The increase was 3.3±0.8 and 11.4±5.3 fold higher in PolgA for both pRPS6 and pS6K1, respectively

(p<0.001, Fig. 4A-C). These data demonstrate that the amino acid leucine increases downstream mTORC1 signaling to a greater extent in PolgA mutated compared to WT muscle. *In vivo*, leucine sensing towards mTORC1 might be altered by the presence of other amino acids or growth factors. To rule out such interference, we cultured myogenic progenitor (MPs) cells from WT and PolgA hind limb muscle to verify proliferation capacity and leucine sensing without the availability of other amino acids. Strikingly, both 5-ethynyl-2'-deoxyuridine (Edu) incorporation and proliferation (Fig. 4D-F) were reduced in PolgA derived MPs. Furthermore, after differentiation, which was unaffected by PolgA mutation (Fig. 4G), we subjected myotubes to varying doses of leucine after 60 min of starvation. In contrast to our *in vivo* data, PolgA myotubes showed a strong anabolic resistance to leucine, as indicated by lower pS6K1 at 0.8mM and 5mM leucine, respectively (Fig. 4H,I). These data show that PolgA muscle progenitors have reduced cell proliferation capacity *in vitro*, potentially due to lower sensitivity to leucine.

*Reduced bone quantity and quality in PolgA mice*

As the results of the cross-sectional experiments described above suggest that PolgA mice display clear signs of co-existing osteopenia and sarcopenia from 40 weeks onwards, we aimed to longitudinally track individual mice during the transition from young to frail status in order to gain a better understanding of when exactly and to what extent bone loss (osteopenia) occurs in individual mice. Therefore, we used an *in vivo* micro-CT approach to monitor the dynamic changes in the bone microarchitecture of the 6$^{th}$ caudal vertebrae (CV6) in individual mice between the ages of 20 and 40 weeks (Fig. 5). The comparison between genotypes showed that at 20 weeks, PolgA and WT had similar trabecular morphometric parameters. Initially, bone volume fraction (BV/TV) and trabecular thickness (Tb.Th) increased in both genotypes, but then started to diverge such that BV/TV and Tb.Th were higher in WT mice from 30 weeks onwards (p<0.05, Fig. 5A,B). Furthermore, from 30 weeks onwards, Tb.Th continuously

increased in WT (+5%, $p<0.0001$), whereas it did not change in PolgA (-1.3%, $p>0.5$, Fig. 5B). No significant differences between genotypes were detected for the trabecular number (Tb.N) and separation (Tb.Sp, Fig. 5C,D). Nevertheless, Tb.N in WT decreased between 30 and 40 weeks (-2.5%, $p<0.05$), whereas Tb.N did not change over time in PolgA mice (-0.3%, $p>0.05$, Fig. 5C). The reduction in Tb.N together with the increase in Tb.Sp in WT explain the slight decrease in BV/TV in WT mice from 36 weeks onwards. A significant interaction between age and genotype, indicating that the time course developed differently between genotypes, was found for Tb.Th, Tb.N and Tb.Sp.

Similar results were obtained when the cortical bone morphometric parameters were analyzed. At 20 weeks, there were no differences between genotypes in cortical area fraction (Ct.Ar/Tt.Ar), cortical thickness (Ct.Th) and cortical marrow volume (Ct.MV) (Fig. 5E, F, H). The total cross-sectional area (Tt.Ar) was already higher (+6%, $p<0.05$) in WT compared to PolgA at 20 weeks (Fig. 5G) with this difference becoming more accentuated up to 40 weeks (+11%, $p<0.001$). Ct.Th increased over time, but then diverged such that Ct.Th was higher than that of PolgA mice from 32 weeks onwards ($p<0.05$). This resulted in a higher Ct.Ar/Tt.Ar in PolgA mice from 36 weeks onwards ($p<0.05$). No differences in Ct.MV were detected between genotypes. A significant interaction between age and genotype was also found for Ct.Ar/Tt.Ar, Ct.Th, Tt.Ar and Ct.MV. The thickening of the trabecular and cortical structure was also visually apparent from the micro-CT images and can be appreciated when the same cross-section is observed at 20 and 40 weeks (Fig. 5E,J).

*Reduced bone turnover in PolgA mice*

In addition to investigating the changes in bone morphometry over time, we also tracked the dynamic remodeling activities, a read out for bone turnover, of PolgA and WT mice (Fig. 6). On average, PolgA mice had lower bone formation rate (BFR, -23.2%, $p<0.05$) and bone resorption rate (BRR, -28.8%, $p<0.05$) compared to WT (Fig. 6A,B). BFR and BRR changed

over time in both genotypes ($p<0.001$), however the time course did not develop differently between genotypes (interaction effect, $p>0.05$). Hence, the net remodeling rate (BFR-BRR) was not different between genotypes. The mineral apposition and resorption rate (MAR and MRR, respectively), which represent the thickness of formation and resorption packages were lower (-8.9%, $p<0.05$ and -20.1%, $p<0.001$) in PolgA compared to WT (Fig. 6C,D). MAR did not change over time and showed no significant interaction between age and genotype (Fig. 6C). On the other hand, there was a significant interaction effect of age and genotype on MRR ($p<0.05$). Over time, MRR increased in WT, while MRR remained constant in PolgA (Fig. 6D). The mineralized surface (MS), which represents the surface of formation sites, was lower in PolgA (-11.8%, $p<0.0001$), whereas the eroded surface (ES) was similar between genotypes ($p>0.05$) (Fig. 6E,F). MS and ES changed over time in both genotypes, however the time course did not develop differently between genotypes (interaction effect, $p>0.05$). Overall, these results suggest that PolgA mice have reduced bone turnover compared to WT.

*Reduced mechanosensitivity of PolgA caudal vertebrae with age*

To investigate whether prematurely aged PolgA bones are mechanosensitive, the 6$^{th}$ caudal vertebrae were cyclically loaded 3x/week over 4 weeks using a previously developed loading device (*48*). Figure 7 shows the absolute values of trabecular bone morphometric parameters at the end of the mechanical loading intervention in young (A,B) and aged (C,D) mice. At young age, loading elicited an anabolic response both in WT and PolgA mice such that BV/TV and Tb.Th were higher ($p<0.0001$) in the loaded compared to the sham-loaded controls (Fig. 7A,B). Strikingly, the anabolic effect was maintained with age in WT ($p<0.05$), whereas PolgA mice did not respond to the mechanical loading intervention, with no differences detected between loaded and non-loaded controls (Fig. 7C,D).

## Discussion

Due to the accumulation of mitochondrial DNA mutations with age, PolgA mice are known to develop multiple signs of aging (alopecia, greying, hearing loss, kyphosis, reduced bone and muscle mass) early in life (*38, 39*). Here, we used the clinical mouse FI (*33*), which was recently reverse translated from the FI in humans (*32*), to quantify the accumulation of these health deficits over time in individual mice. Furthermore, as the weakening of the musculoskeletal system is a major component of age-related frailty, we used a combination of *in vivo, ex vivo* and *in vitro* techniques to comprehensively characterize the musculoskeletal phenotype of this model. Lastly, the effects of various anabolic interventions on the musculoskeletal system of PolgA mice were assessed.

This study demonstrated that in comparison to their chronologically aged WT littermates, PolgA mice developed many hallmarks of aging over time which collectively resulted in PolgA mice becoming frailer with age. Of the 31 items included in the FI scoring, changes in the integument category were the most striking. Specifically, PolgA mice showed a loss in fur color (from black to grey/brown) and a decline in the coat condition (ruffled fur, ungroomed appearance). Furthermore, they showed signs of enlarged abdomen and kyphosis. At 40 weeks of age (280 days), PolgA mice had mean frailty scores of 0.15±0.02 (mean±SD), whereas WT mice had 0.06±0.04, respectively. A previous study using male C57BL/6J mice reported mean FI values of 0.05±0.05 in young (30-299 days), 0.21±0.04 in middle-aged (300-599 days) and 0.29±0.07 in older mice (above 600 days) (*34*). Comparing these values to the ones observed in our study, the (female) WT mice (at 40 weeks < 299 days) fall in the category of young mice, whereas the PolgA mice fall into the category of “middle-aged” mice. Although some studies have reported higher FI scores in female compared to male mice (*33, 49*), others showed no differences in frailty between sexes (*50, 51*); furthermore, it seems that the rate of deficit accumulation is similar between sexes (*49*). Nevertheless, future studies in which PolgA mice

are aged for a longer period of time (>300 days) would be necessary to investigate the degree of frailty at later stages in life. Our ethical permit for breeding was constrained to a maximum of 46 weeks as previous studies reported median lifespans of PolgA mice ranging from ca. 59 weeks (416 days) (*38*), 48 weeks (336 days) (*39*), down to only 36 weeks (250 days) (*41*). The discrepancies between studies regarding the lifespan is also apparent for the age at which symptoms of aging first appeared (ranging from 6- (*41*) to 9 months (*38, 39*)). As not only homozygous (PolgA$^{D257A/D257A}$), but also heterozygous (PolgA$^{D257A/+}$) mice progressively accumulate mitochondrial DNA point mutations with age, we suspect that the differences between studies resulted from differences in breeding schemes. Since all the mice used in our study were bred according to a standardized breeding scheme, thereby displaying only a single generation of mutation burden, the onset of the accelerated aging phenotype may have been delayed in the present work as compared to other studies. Nevertheless, we observed that PolgA mice became frailer faster than WT, as shown by plotting the natural logarithm of the FI as a function of age and fitting the resulting relationship with a linear function. This approach has previously been used to illustrate the rate of deficit accumulation in studies of older humans (*44*). In the study by Rockwood et al. (*34*), this slope has been shown to be slightly higher with a value of 0.036 compared to our value of 0.025. Nevertheless, the value shown in humans is similar to ours (0.029). To our knowledge, we are the first to report the frailty phenotyping in the PolgA mouse model.

In line with increased FI with age, the musculoskeletal phenotype clearly diverged over time between genotypes, with PolgA mice developing multiple signs of osteosarcopenia with age. In agreement with previous reports showing lower muscle weights (*38, 40, 41*) and reduced femoral bone mineral density assessed by X-ray densitometry (*38, 39*), phenotyping of the femora and hind limb muscles revealed lower bone and muscle mass as well as cross-sectional area in PolgA mice compared to their WT littermates at 40 and 46 weeks of age. These

reductions were not observed at 34 weeks, thus indicating a progressive weakening of the musculoskeletal system in the PolgA mice. As the clinical diagnosis of sarcopenia is not only characterized by reduced muscle mass but also by reduced muscle function and quality, we assessed the forelimb grip-strength, muscle force and intramuscular signaling upon anabolic stimuli. In agreement with clinically diagnosed sarcopenia, PolgA displayed lowered muscle strength, indicated by reduced grip-strength and lower concentric contraction force at different intensities.

One mechanism commonly thought of as a contributor to sarcopenia is the age-related lowered sensitivity to anabolic stimuli. This phenomenon, known as anabolic resistance, has been associated with the reduced acute activation of mTORC1 (*13-15*), the central protein complex that integrates external stimuli to regulate cell growth (*52-55*). Note that the interpretation of the data described in previous studies, which showed increased anabolic resistance upon heavy-load contractions, might be confounded by the fact that the same relative load (% 1 repetition max) was used in old vs. young humans (*13*). The lower absolute load in the aged subjects might have caused lower mechanical stress on the muscle, as demonstrated by lower MAPK signaling (*56*), and thus a dampened increase in mTORC1 signaling. By using the protocol described by O'Neil et al. (*57*), we could overcome this confounding factor by controlling the load applied to the muscles. Interestingly, although the average force produced during the 60 contractions was similar between WT and PolgA, both MAPK and downstream mTORC1 signaling was remarkably elevated in PolgA mutated muscle. Notably, leucine also activated mTORC1 to a greater extent in 46-week-old PolgA muscle compared to their chronologically aged WT littermates. This is intriguing as eccentric contractions and leucine independently activate mTORC1 signaling (*58*). Both increased mechanical stress and elevated reactive oxygen species (*59, 60*) could be responsible, but further research is needed to fully elucidate the mechanisms behind mTORC1 hyperactivity in PolgA muscle. Nevertheless, this is the first

time mTORC1 hyperactivity is shown upon anabolic stimuli in accelerated aged muscle and adds to the notion that mTORC1 hyperactivity might be deleterious to long term muscle health.

*In vivo*, the systemic availability of amino acids/nutrients and differences in the local niche might have interfered with hyperactive mTORC1 signaling in PolgA. To rule this out, we used an *in vitro* approach to study the activation of mTORC1 in MPs that were stimulated with identical concentrations of leucine, without the availability of other amino acids. We were able to demonstrate that PolgA primary MPs had substantial defects in proliferative capacity and were completely insensitive to leucine with respect to mTORC1 anabolic signaling. Thus, it seems that mitochondrial dysfunction per se is sufficient to induce impairments in muscle stem cell mTORC1 signaling, regardless of exposure to the local niche. The differences in downstream mTORC1 signaling upon anabolic signals between whole muscle and their respective stem cells are puzzling, but can potentially be induced by the higher accumulation of mitochondrial damage under proliferative *in vitro* conditions when compared to post mitotic differentiated muscle tissue that develops apoptosis at a later stage (*38*). Nonetheless, these data warrant caution in the translation of MP-derived experimental data to the *in vivo* muscle setting and suggest that the accumulation of mitochondrial damage is tissue specific and can profoundly change the mTORC1 response to leucine.

With respect to the evaluation of the bone phenotype, this study is to the best of our knowledge, the first to use standardized micro-CT approaches to comprehensively characterize the bone phenotype of the PolgA mouse model (*42, 43, 61*). Albeit still considered the clinical gold standard for assessing bone mineral density in humans, X-ray densitometry, which was previously used to evaluate the PolgA bone phenotype (*38, 39*), is confounded by the size and positioning of the bone, and furthermore, does not provide any information on the bone microarchitecture (*62, 63*). Nevertheless, the results of this study did recapitulate the clear reductions measured in femoral bone mineral density in PolgA mice with age (*38, 39*). Note

that the accuracy of the aforementioned phenotyping of the femora, both in the previous as well as in the current study, is limited by the cross-sectional study design. This type of study design cannot account for the intrinsic initial variability between animals at baseline (*64, 65*), thereby making it impossible to determine the amount of bone lost in individual mice. We therefore used an established *in vivo* micro-CT approach to monitor the spatio-temporal changes in bone micro-architecture in the caudal vertebrae of individual mice during the transition from healthy to frail state. Multiple bone morphometric parameters diverged over time, from being similar at 20 weeks to lower in PolgA mice with age. Interestingly though, this difference did not arise due to significant bone loss in PolgA mice, but rather in the failure to achieve normal peak bone mass. We and others have previously reported the absence of age-related bone loss in caudal vertebrae (*66, 67*). Hence, mouse caudal vertebrae may not be suitable for investigating age-related bone loss. Indeed, a more severe age-related deterioration of trabecular bone microarchitecture in long bones compared to lumbar vertebrae has previously been reported in a cross-sectional study in aged C57Bl/6J mice (*65*); hence, monitoring the long bones of PolgA mice by *in vivo* micro-CT may be beneficial in future studies. Beyond enhanced phenotyping, the current study capitalized on the ability of *in vivo* micro-CT to provide information on the dynamic coupling between bone resorption and formation. Compared to WT littermates, PolgA had lower bone turnover as shown by reduced bone formation and resorption rates, with no differences in the net remodeling rate. Similarly, senile osteoporosis in humans is characterized by low bone turnover, as opposed to the high bone turnover rates (higher resorption activities) observed during postmenopausal osteoporosis. Despite the advantages of *in vivo* micro-CT, the anesthesia, cumulative radiation, and stress associated with repeated CT measurements could have an effect on the bone morphometry and the well-being of the animals (*68-72*). However, as effects of radiation are of greater concern in young, growing mice, and furthermore, have been shown to be independent of surgical treatments (e.g., ovariectomy) (*68*), we suspect that any effects of radiation would be similar in WT and PolgA mice. Nevertheless, we compared

the bone remodeling activities of PolgA and WT mice used in this study (subjected to 11 *in vivo* measurements) with those of corresponding age-matched controls that received only 2 *in vivo* scans at 38 and 40 weeks, respectively, and saw no statistical differences between the groups. Furthermore, we did not observe any negative effects of any of these variables on the well-being of the animals.

Finally, after having established that PolgA mutation altered the sensitivity to anabolic stimuli in muscles and their progenitors, we also investigated the responsiveness of PolgA bones to an established mechanical loading regime (*73*). Interestingly, PolgA mice were not responsive to cyclic loading of the caudal vertebrae over 4 weeks, whereas loading had beneficial effects in WT mice. Although there are controversial reports on the maintenance of bone mechanosensitivity with age in mice (*27-30*), these results conflicted with our previous observation that caudal vertebrae remain mechanosensitive to cyclic mechanical loading with age (*31*). Interestingly, in the previous study, 82-week-old C57BL/6J mice showed a greater anabolic response compared to the 52-week old group; hence, the response of PolgA mice over 46 weeks of age may be different than those used in this study. Furthermore, the load in this study was not adjusted to account for differences in the initial bone volume fraction between PolgA and WT mice. An individualized loading approach, which ensures that all bones are subjected to the same mechanical strain, could yield differences in the mechanosensitivity of the PolgA and WT mice. Nevertheless, adapting the loading for the lower bone mass in the PolgA would decrease the stimulus and therefore, we do not expect a positive response at this even lower stimulus. Nonetheless, further research is therefore needed to elucidate the mechanosensitivity of PolgA bones.

In conclusion, we show that PolgA mice develop multiple hallmarks of aging, such as reduced bone turnover and muscle mass early in life, which collectively can be quantified using the mouse FI. We further demonstrate mTORC1 hyperactivity in PolgA muscle upon anabolic

signals, which is related to diminished satellite cell proliferation. By mimicking many aspects of osteosarcopenia, the PolgA mouse provides a powerful model that facilitates our understanding of the relationship between muscles and bones, and also between the aging musculoskeletal system and frailty.

## Materials and Methods

### *Study Design*

The study consisted of three parts. For parts 1 and 2, female mice were aged up to 46 weeks and divided into four groups. Three of the groups were used to cross-sectionally compare the musculoskeletal and frailty phenotype of PolgA and WT mice at 34, 40 and 46 weeks, respectively (*in vivo* and *ex vivo*, part 1). The fourth group was longitudinally monitored between the ages of 20 and 40 weeks to investigate the changes in bone microarchitecture and frailty over time (*in vivo*, part 2). Lastly, the effects of various anabolic interventions on bone and muscle tissue were assessed (*in vivo*, *ex vivo*, *in vitro*). The number of mice and sample sizes in various animal studies are provided directly in the figure legends and in table S1. The sample sizes for *in vivo* experiments were selected based on previous experiments and power analysis (power set at 0.80) was used to determine the sample size required for *ex vivo* experiments. All mouse experiments described in the present study were carried out in strict accordance with the recommendations and regulations in the Animal Welfare Ordinance (TSchV 455.1) of the Swiss Federal Food Safety and Veterinary Office and results are reported following the principles of the ARRIVE guidelines (www.nc3rs.org.uk/arrive-guidelines).

### *Animals*

All animal procedures were approved by the local authorities (licence numbers 262/2016 and ZH255-16, Verterinäramt des Kantons Zürich, Zurich, Switzerland). A colony of the mouse strain expressing an exonuclease-deficient version of the mitochondrial DNA polymerase γ

(PolgA$^{D257A}$, B6.129S7(Cg)-Polg$^{tm1Prol}$/J, JAX stock 017341, The Jackson Laboratory) was bred and maintained at the ETH Phenomics Center (12h:12h light-dark cycle, maintenance feed and water ad libitum, 3-5 animals/cage). The mice were bred and genotyped as described in Supplementary Materials (SM). In order to confirm that the premature aging phenotypes were associated with mitochondrial dysfunction, the activity of complex IV enzyme (COX IV) in *m. gastrocnemius* (GAS) was measured (SM). Compared to WT, PolgA muscles had lower COX IV activity both at 40 and 46 weeks (-19% and -24%, $p<0.0001$, respectively), thus confirming that the mice used in this study had the same phenotype as those previously reported (*40, 41, 74*).

*Quantification of Frailty Index (FI)*

Frailty was quantified using the Mouse Clinical FI (*33*), which includes the assessment of 31 non-invasive clinical items. For 29 of these items, mice were given a score of 0 if not present, 0.5 if there was a mild deficit, and 1 for a severe deficit. The final two items were weight and body surface temperature, which were scored based on the number of standard deviations from a reference mean in young adult mice as previously described (*33*). To compare rates of deficit accumulation between PolgA and WT, the natural log of the FI was plotted against age. The slope of this line provides an estimate of the rate of deficit accumulation, as shown in previous studies (*33, 44, 75*).

*Forelimb Grip-Strength*

Forelimb grip-strength was measured using a force tension apparatus (Grip Strength Meter, 47200, Ugo Basile) at 40 and 46 weeks of age. Once mice gripped the stationary bar with their forepaws, they were pulled horizontally at the base of their tail until they let go of the bar. The process was repeated 5 times to determine the average peak grip force value (gram-force) used for analysis. All measurements were performed by the same experienced user.

*Muscle harvesting and force measurements*

PolgA and WT GAS, TA and *m. soleus* (SOL) were excised under anesthesia (5% isoflurane/oxygen) and snap frozen in liquid nitrogen. Furthermore, EDL from both legs were dissected and maintained in 4°C Krebs–Henseleit buffer supplemented with 1×MEM amino acid mixture (Invitrogen) and 25mM glucose. For assessment of *ex vivo* force production, the EDL of the right leg was attached to the lever arms of an Aurora system (Aurora Scientific) and submerged in continuously gassed Krebs–Henseleit buffer maintained at 37°C. After 5 min of temperature acclimation, muscle length was adjusted until a single stimulus pulse elicited maximum force during a twitch (Lo) under isometric conditions. After 5 min rest, a force frequency protocol was initiated by subsequently providing a pulse train (lasting 250 ms) of 1-30-50-80-150-250 and 300Hz with 1 min rest between every intensity.

*Eccentric contractions (ECC) protocol*

5 min after the force frequency protocol, EDL from the right legs were subjected to an eccentric training protocol according to O'Neil et al. (*57*) consisting of 60 contractions in a 22 min time window. In this study, the pulse train was changed to 200Hz (compared to 100Hz in O'Neil et al.), because pilot studies suggested that 100Hz was not sufficient to induce maximal eccentric force in older muscle. After the contractions, the muscle was maintained in 37°C Krebs–Henseleit buffer + 1xMEM amino acid mixture and 25mM glucose before snap-freezing 1h after the last contraction. The control EDL from the contralateral leg was kept in the same 37°C Krebs–Henseleit buffer during the complete ECC period.

*Leucine administration*

46 week-old mice were fasted for 5h in the beginning of their light cycle, after which saline (0.9% NaCl, CTL) or leucine (0.4g/kg, LEU) was administered via oral gavage. L-Leucine (Sigma Aldrich) was dissolved in a stock solution of 40g/L, heated (40-50°C) and acidified as

described previously (*76*). 30 min later, hind limb muscles were weighted and snap frozen for further analysis.

*Leucine stimulation in vitro*

Primary muscle progenitor cells (MPs) were isolated from muscle tissue as described in SM. 200'000 cells were seeded in 6-well-plates. Myogenic differentiation medium containing low-glucose DMEM, 2% Horse-serum (HS) (Invitrogen) and 1% P/S was added 24h later. 72h later, fully differentiated MPs were treated according to one of the following conditions: (1) STV; 1h DMEM w/o amino acids (Biomol GmbH) + 10% dialyzed FBS (Invitrogen) + 1% P/S, (2) LEU 0.8; 1h STV + 1h 0.8mM L-Leucine (Sigma Aldrich) and (3) LEU 5; 1h STV + 1h 5mM L-Leucine. Experiments were performed in biological triplicate and technical duplicate. Edu analysis was performed according to manufacturer's protocol (Thermo Fischer Scientific) after a 4h pulse with 1µg/ml Edu. For proliferation analysis, 20'000 cells were plated on 12-well-plates, and 3 plates were counted per time point over 5 days.

*Immunoblotting*

Details have been described previously (*77*) and are further described in SM.

*Micro-CT imaging and analysis*

For analysis of femoral, the right femora were harvested, placed in 70% Ethanol and scanned with micro-CT (micro-CT40, Scanco Medical AG, isotropic nominal resolution: 10 µm; 55 kVp, 145 µA, 200 ms integration time). A 3D constrained Gaussian filter (sigma 1.2, support 1) was applied to the image data, after which images were segmented by a global thresholding procedure (*78*). Standard bone microstructural parameters were calculated in trabecular (BV/TV, Tb.Th, Tb.N, Tb.Sp), cortical (Tt.Ar, Ct.Ar/Tt.Ar, Ct.MV) and whole (AVD, length) bone using automatically selected masks for these regions (*61*).

For analysis of the 6th caudal vertebra (CV6), *in vivo* micro-CT (vivaCT 40, Scanco Medical AG, isotropic nominal resolution: 10.5 µm; 2 stacks of 211 slices; 55 kVp, 145 µA, 350 ms integration time, 500 projections per 180°, scan duration ca. 15 min, radiation dose per scan ca. 640 mGy) was performed every 2 weeks between 20 and 40 weeks of age. Animals were anesthetized with isoflurane (induction/maintenance: 5%/1-2% isoflurane/oxygen). Micro-CT data was processed and standard bone microstructural parameters were calculated in trabecular, cortical and whole bone by using automatically selected masks for these regions as described previously (*73*).

To calculate dynamic morphometric parameters, micro-CT images from consecutive time-points were registered onto one another. The voxels present only at the initial time point were considered resorbed whereas voxels present only at the later time point were considered formed. Voxels that were present at both time points were considered as quiescent bone. By overlaying the images, morphometrical analysis of bone formation and resorption sites within the trabecular region allowed calculations of bone formation rate (BFR), bone resorption rate (BRR), mineral apposition rate (MAR), mineral resorption rate (MRR), mineralizing surface (MS) and eroded surface (ES) (*43*).

*Cyclic mechanical loading of CV6*

CV6 were subjected to a cyclic loading regime, which has previously been shown to have anabolic effects in 15-week-old female C57BL/6J mice (*48*). Briefly, stainless steel pins (Fine Science Tools) were inserted into the 5th and 7th caudal vertebrae of 35- and 12-week old female mice. Three weeks after surgery, the mice received either sham (0N control) or 8N cyclic (10 Hz) loading for 5 minutes, 3x/week over 4 weeks. Weekly *in vivo* micro-CT images were acquired and analyzed as described above.

*Statistical analysis*

Data is reported as mean and standard error of the mean (±SEM), unless otherwise stated. All analysis, with the exception of the longitudinal micro-CT data, was performed using GraphPadPrism (8.0.0). Unpaired or paired Student's t-test, one- or two-way ANOVA with post hoc multiple comparison testing were performed as indicated in figure legends. For the analysis of the longitudinal micro-CT data, linear mixed-effects modelling was used with Tukey's post hoc multiple comparison testing corrected with Bonferroni criteria (SPSS 24.0.0.0). Fixed-effects were allocated to the age and genotype. Random-effects were allocated to the animal to account for the natural differences in bone morphometry in different mice. Significance was set at $\alpha<0.05$ in all experiments.

**Supplementary Materials**

Materials and Methods

Table S1. Animal experiments: Overview, setup and analysis details.

550 **References and Notes**


551 1. Rodríguez-Mañas L, Gonzalez-Colaço Harmand M, Carcaillon L, Scuteri A, Sinclair
552 A, Pelaez M, Van der Cammen T, Beland F, Bickenbach J, Delamarche P, Ferrucci L,
553 Fried LP, Gutiérrez-Robledo LM, Féart C, Rockwood K, Rodríguez Artalejo F,
554 Serviddio G, Vega E, Nicholson C, Mann G, Viña J, Chatterji S, Chodzko-Zajko W,
555 Bergman H. Searching for an operational definition of frailty: a delphi method based
556 consensus statement. The Frailty Operative Definition-Consensus Conference Project.
557 J Gerontol A Biol Sci Med Sc, 2013; 68(1):62-67.

558 2. Whitson HE, Duan-Porter W, Schmader KE, Morey MC, Cohen HJ, Colon-Emeric CS.
559 Physical resilience in older adults: systematic review and development of an emerging
560 construct. J Gerontol A 2016; 71(4):489-495.

561 3. McGuigan FE, Bartosch P, Åkesson KE. Musculoskeletal health and frailty. Best Pract
562 Res Clin Rheumatol, 2017; 31(2):145-159.

563 4. Milte R,Crotty M. Musculoskeletal health, frailty and functional decline. Best Pract Res
564 Clin Rheumatol, 2014; 28(3):395-410.

565 5. Frisoli A, Chaves PH, Ingham SJM, Fried LP. Severe osteopenia and osteoporosis,
566 sarcopenia, and frailty status in community-dwelling older women: results from the
567 Women's Health and Aging Study (WHAS) II. Bone, 2011; 48(4):952-957.

568 6. Hassan E,Duque G. Osteosarcopenia: a new geriatric syndrome. Australian Family
569 Physician, 2017; 46:849-853.

570 7. Hirschfeld HP, Kinsella R, Duque G. Osteosarcopenia: where bone, muscle, and fat
571 collide. Osteoporos Int, 2017; 28(10):2781-2790.

572 8. Yu R, Leung J, Woo J. Incremental predictive value of sarcopenia for incident fracture
573 in an elderly Chinese cohort: results from the Osteoporotic Fractures in Men (MrOs)
574 Study. J Am Med Dir Assoc, 2014; 15(8):551-558.

575 9. Huo YR, Suriyaarachchi P, Gomez F, Curcio CL, Boersma D, Gunawardene P,
576 Demontiero O, Duque G. Comprehensive nutritional status in sarco-osteoporotic older
577 fallers. J Nutr Health Aging, 2015; 19(4):474-480.
578 10. van Dijk M, Nagel J, Dijk FJ, Salles J, Verlaan S, Walrand S, van Norren K, Luiking
579 Y. Sarcopenia in older mice is characterized by a decreased anabolic response to a
580 protein meal. Arch Gerontol Geriatr, 2017; 69:134-143.
581 11. Chalil S, Pierre N, Bakker AD, Manders RJ, Pletsers A, Francaux M, Klein-Nulend J,
582 Jaspers RT, Deldicque L. Aging related ER stress is not responsible for anabolic
583 resistance in mouse skeletal muscle. Biochem Biophys Res Commun, 2015;
584 468(4):702-707.
585 12. Katsanos CS, Kobayashi H, Sheffield-Moore M, Aarsland A, Wolfe RR. Aging is
586 associated with diminished accretion of muscle proteins after the ingestion of a small
587 bolus of essential amino acids. Am J Clin Nutr, 2005; 82(5):1065-1073.
588 13. Fry CS, Drummond MJ, Glynn EL, Dickinson JM, Gundermann DM, Timmerman KL,
589 Walker DK, Dhanani S, Volpi E, Rasmussen BB. Aging impairs contraction-induced
590 human skeletal muscle mTORC1 signaling and protein synthesis. Skelet Muscle, 2011;
591 1(1):11.
592 14. Francaux M, Demeulder B, Naslain D, Fortin R, Lutz O, Caty G, Deldicque L. Aging
593 reduces the activation of the mTORC1 pathway after resistance exercise and protein
594 intake in human skeletal muscle: potential role of REDD1 and impaired anabolic
595 sensitivity. Nutrients, 2016; 8(1).
596 15. Cuthbertson D, Smith K, Babraj J, Leese G, Waddell T, Atherton P, Wackerhage H,
597 Taylor PM, Rennie MJ. Anabolic signaling deficits underlie amino acid resistance of
598 wasting, aging muscle. FASEB J, 2005; 19(3):422-424.

599 16. Breen L,Phillips SM. Skeletal muscle protein metabolism in the elderly: interventions
600 to counteract the 'anabolic resistance' of ageing. Nutr Metab (Lond), 2011; 8:68.
601 17. Guillet C, Prod'homme M, Balage M, Gachon P, Giraudet C, Morin L, Grizard J, Boirie
602 Y. Impaired anabolic response of muscle protein synthesis is associated with S6K1
603 dysregulation in elderly humans. FASEB J, 2004; 18(13):1586-1587.
604 18. Symons TB, Schutzler SE, Cocke TL, Chinkes DL, Wolfe RR, Paddon-Jones D. Aging
605 does not impair the anabolic response to a protein-rich meal. Am J Clin Nutr, 2007;
606 86(2):451-456.
607 19. Symons TB, Sheffield-Moore M, Wolfe RR, Paddon-Jones D. A moderate serving of
608 high-quality protein maximally stimulates skeletal muscle protein synthesis in young
609 and elderly subjects. Journal of the American Dietetic Association, 2009; 109(9):1582-
610 1586.
611 20. Symons TB, Sheffield-Moore M, Mamerow MM, Wolfe RR, Paddon-Jones D. The
612 anabolic response to resistance exercise and a protein-rich meal is not diminished by
613 age. J Nutr Health Aging, 2011; 15(5):376-381.
614 21. Nederveen JP, Joanisse S, Snijders T, Ivankovic V, Baker SK, Phillips SM, Parise G.
615 Skeletal muscle satellite cells are located at a closer proximity to capillaries in healthy
616 young compared with older men. J Cachexia Sarcopenia Muscle, 2016; 7(5):547-554.
617 22. Verdijk LB, Koopman R, Schaart G, Meijer K, Savelberg HHCM, van Loon LJC.
618 Satellite cell content is specifically reduced in type II skeletal muscle fibers in the
619 elderly. Am J Physiol Endocrinol Metab, 2007; 292(1):E151-E157.
620 23. Barberi L, Scicchitano BM, De Rossi M, Bigot A, Duguez S, Wielgosik A, Stewart C,
621 McPhee J, Conte M, Narici M, Franceschi C, Mouly V, Butler-Browne G, Musaro A.
622 Age-dependent alteration in muscle regeneration: the critical role of tissue niche.
623 Biogerontology, 2013; 14(3):273-292.

624 24. Parker MH. The altered fate of aging satellite cells is determined by signaling and
625 epigenetic changes. Frontiers in genetics, 2015; 6:59-59.
626 25. Yin H, Price F, Rudnicki MA. Satellite cells and the muscle stem cell niche. Physiol
627 Rev, 2013; 93(1):23-67.
628 26. Stattin K, Michaëlsson K, Larsson SC, Wolk A, Byberg L. Leisure-time physical
629 activity and risk of fracture: a cohort study of 66,940 men and women. J Bone Miner
630 Res, 2017; 32(8):1599-1606.
631 27. Lynch ME, Main RP, Xu Q, Schmicker TL, Schaffler MB, Wright TM, van der Meulen
632 MCH. Tibial compression is anabolic in the adult mouse skeleton despite reduced
633 responsiveness with aging. Bone, 2011; 49(3):439-446.
634 28. Willie BM, Birkhold AI, Razi H, Thiele T, Aido M, Kruck B, Schill A, Checa S, Main
635 RP, Duda GN. Diminished response to in vivo mechanical loading in trabecular and not
636 cortical bone in adulthood of female C57Bl/6 mice coincides with a reduction in
637 deformation to load. Bone, 2013; 55(2):335-346.
638 29. Birkhold AI, Razi H, Duda GN, Weinkamer R, Checa S, Willie BM. Mineralizing
639 surface is the main target of mechanical stimulation independent of age: 3D dynamic in
640 vivo morphometry. Bone, 2014; 66:15-25.
641 30. Holguin N, Brodt MD, Sanchez ME, Silva MJ. Aging diminishes lamellar and woven
642 bone formation induced by tibial compression in adult C57BL/6. Bone, 2014; 65:83-91.
643 31. Lambers FM, Kuhn G, Weigt C, Koch KM, Schulte FA, Müller R. Bone adaptation to
644 cyclic loading in murine caudal vertebrae is maintained with age and directly correlated
645 to the local micromechanical environment. J Biomech, 2015; 48(6):1179-1187.
646 32. Jones DM, Song XW, Rockwood K. Operationalizing a frailty index from a
647 standardized comprehensive geriatric assessment. J Am Geriatr Soc, 2004;
648 52(11):1929-1933.

649 33. Whitehead JC, Hildebrand BA, Sun M, Rockwood MR, Rose RA, Rockwood K,
650 Howlett SE. A clinical frailty index in aging mice: comparisons with frailty index data
651 in humans. J Gerontol A Biol Med Sci, 2014; 69(6):621-632.
652 34. Rockwood K, Blodgett JM, Theou O, Sun MH, Feridooni HA, Mitnitski A, Rose RA,
653 Godin J, Gregson E, Howlett SE. A frailty index based on deficit accumulation
654 quantifies mortality risk in humans and in mice. Sci Rep, 2017; 7:43068.
655 35. Banga S, Heinze-Milne SD, Howlett SE. Rodent models of frailty and their application
656 in preclinical research. Mech Ageing Dev, 2019; 179:1-10.
657 36. Trendelenburg AU, Scheuren AC, Potter P, Müller R, Bellantuono I. Geroprotectors: a
658 role in the treatment of frailty. Mech Ageing Dev, 2019; 180:11-20.
659 37. I. Bellantuono RD, D. Ehninger, A. Fernandes, S. E. Howlett, R. Müller, P. Potter, T.
660 Tchkonia, A.-U. Trendelenburg, J. L. Trejo, R. Vandenbroucke, R. van Os, N. van Riel.
661 Find drugs that delay many diseases of old age. Nature, 2018; 554:293-295.
662 38. Kujoth GC, Hiona A, Pugh TD, Someya S, Panzer K, Wohlgemuth SE, Hofer T, Seo
663 AY, Sullivan R, Jobling WA, Morrow JD, Van Remmen H, Sedivy JM, Yamasoba T,
664 Tanokura M, Weindruch R, Leeuwenburgh C, Prolla TA. Mitochondrial DNA
665 Mutations, Oxidative Stress, and Apoptosis in Mammalian Aging. Science, 2005;
666 309(5733):481.
667 39. Trifunovic A, Wredenberg A, Falkenberg M, Spelbrink JN, Rovio AT, Bruder CE,
668 Bohlooly YM, Gidlof S, Oldfors A, Wibom R, Tornell J, Jacobs HT, Larsson NG.
669 Premature ageing in mice expressing defective mitochondrial DNA polymerase. Nature,
670 2004; 429(6990):417-423.
671 40. Kolesar JE, Safdar A, Abadi A, MacNeil LG, Crane JD, Tarnopolsky MA, Kaufman
672 BA. Defects in mitochondrial DNA replication and oxidative damage in muscle of
673 mtDNA mutator mice. Free Radic Biol Med, 2014; 75:241-251.

674 41. Safdar A, Bourgeois JM, Ogborn DI, Little JP, Hettinga BP, Akhtar M, Thompson JE,
675 Melov S, Mocellin NJ, Kujoth GC, Prolla TA, Tarnopolsky MA. Endurance exercise
676 rescues progeroid aging and induces systemic mitochondrial rejuvenation in mtDNA
677 mutator mice. P Natl Acad Sci USA, 2011; 108(10):4135-4140.
678 42. Bouxsein ML, Boyd SK, Christiansen BA, Guldberg RE, Jepsen KJ, Muller R.
679 Guidelines for assessment of bone microstructure in rodents using micro-computed
680 tomography. J Bone Miner Res, 2010; 25(7):1468-1486.
681 43. Schulte FA, Lambers FM, Kuhn G, Müller R. In vivo micro-computed tomography
682 allows direct three-dimensional quantification of both bone formation and bone
683 resorption parameters using time-lapsed imaging. Bone, 2011; 48(3):433-442.
684 44. Mitnitski A,Rockwood K. Frailty in relation to the accumulation of deficits. J Gerontol
685 A Biol Sci Med Sc, 2007; 62(7):722-727.
686 45. Jacobs BL, You JS, Frey JW, Goodman CA, Gundermann DM, Hornberger TA.
687 Eccentric contractions increase the phosphorylation of tuberous sclerosis complex-2
688 (TSC2) and alter the targeting of TSC2 and the mechanistic target of rapamycin to the
689 lysosome. J Physiol, 2013; 591(18):4611-4620.
690 46. Ogasawara R, Jensen TE, Goodman CA, Hornberger TA. Resistance Exercise-Induced
691 Hypertrophy: A Potential Role for Rapamycin-Insensitive mTOR. Exerc Sport Sci Rev,
692 2019.
693 47. Rahnert JA,Burkholder TJ. High-frequency electrical stimulation reveals a p38-mTOR
694 signaling module correlated with force-time integral. J Exp Biol, 2013; 216(Pt
695 14):2619-2631.
696 48. Webster DJ, Morley PL, van Lenthe GH, Muller R. A novel in vivo mouse model for
697 mechanically stimulated bone adaptation - a combined experimental and computational
698 validation study. Comput Methods Biomech Biomed Engin, 2008; 11(5):435-441.

699 49. Kane AE, Shin S, Wong AA, Fertan E, Faustova NS, Howlett SE, Brown RE. Sex
700 Differences in Healthspan Predict Lifespan in the 3xTg-AD Mouse Model of
701 Alzheimer's Disease. Front Aging Neurosci, 2018; 10.
702 50. Parks RJ, Fares E, MacDonald JK, Ernst MC, Sinal CJ, Rockwood K, Howlett SE. A
703 Procedure for creating a frailty index based on deficit accumulation in aging mice. J
704 Gerontol A Biol Med Sci, 2012; 67(3):217-227.
705 51. Kane AE, Hilmer SN, Boyer D, Gavin K, Nines D, Howlett SE, de Cabo R, Mitchell
706 SJ. Impact of Longevity Interventions on a Validated Mouse Clinical Frailty Index. J
707 Gerontol A Biol Sci Med Sc, 2015; 71(3):333-339.
708 52. Laplante M,Sabatini DM. mTOR signaling in growth control and disease. Cell, 2012;
709 149(2):274-293.
710 53. Yoon M-S. mTOR as a Key Regulator in Maintaining Skeletal Muscle Mass. Frontiers
711 in Physiology, 2017; 8:788.
712 54. Schiaffino S, Dyar KA, Ciciliot S, Blaauw B, Sandri M. Mechanisms regulating skeletal
713 muscle growth and atrophy. The FEBS Journal, 2013; 280(17):4294-4314.
714 55. Hornberger TA, Sukhija KB, Chien S. Regulation of mTOR by Mechanically Induced
715 Signaling Events in Skeletal Muscle. Cell Cycle, 2006; 5(13):1391-1396.
716 56. Williamson D, Gallagher P, Harber M, Hollon C, Trappe S. Mitogen-activated protein
717 kinase (MAPK) pathway activation: effects of age and acute exercise on human skeletal
718 muscle. J Physiol, 2003; 547(Pt 3):977-987.
719 57. O'Neil TK, Duffy LR, Frey JW, Hornberger TA. The role of phosphoinositide 3-kinase
720 and phosphatidic acid in the regulation of mammalian target of rapamycin following
721 eccentric contractions. J Physiol-London, 2009; 587(14):3691-3701.

722 58. Drummond MJ,Rasmussen BB. Leucine-enriched nutrients and the regulation of
723 mammalian target of rapamycin signalling and human skeletal muscle protein synthesis.
724 Curr Opin Clin Nutr, 2008; 11(3):222-226.
725 59. Perez de Obanos MP, Lopez-Zabalza MJ, Arriazu E, Modol T, Prieto J, Herraiz MT,
726 Iraburu MJ. Reactive oxygen species (ROS) mediate the effects of leucine on translation
727 regulation and type I collagen production in hepatic stellate cells. Biochim Biophys
728 Acta, 2007; 1773(11):1681-1688.
729 60. Ahlqvist KJ, Hamalainen RH, Yatsuga S, Uutela M, Terzioglu M, Gotz A, Forsstrom
730 S, Salven P, Angers-Loustau A, Kopra OH, Tyynismaa H, Larsson NG, Wartiovaara K,
731 Prolla T, Trifunovic A, Suomalainen A. Somatic progenitor cell vulnerability to
732 mitochondrial DNA mutagenesis underlies progeroid phenotypes in Polg mutator mice.
733 Cell Metab, 2012; 15(1):100-109.
734 61. Kohler T, Stauber M, Donahue LR, Muller R. Automated compartmental analysis for
735 high-throughput skeletal phenotyping in femora of genetic mouse models. Bone, 2007;
736 41(4):659-667.
737 62. Gasser JA. Assessing bone quantity by pQCT. Bone, 1995; 17(4, Supplement):S145-
738 S154.
739 63. Rosen HN, Tollin S, Balena R, Middlebrooks VL, Beamer WG, Donohue LR, Rosen
740 C, Turner A, Holick M, Greenspan SL. Differentiating between orchiectomized rats and
741 controls using measurements of trabecular bone density: A comparison among DXA,
742 Histomorphometry, and peripheral quantitative computerized tomography. Calcified
743 Tissue Int, 1995; 57(1):35-39.
744 64. Silva MJ, Brodt MD, Lynch MA, Stephens AL, Wood DJ, Civitelli R. Tibial loading
745 increases osteogenic gene expression and cortical bone volume in mature and middle-
746 aged mice. PloS One, 2012; 7(4):e34980.

65. Glatt V, Canalis E, Stadmeyer L, Bouxsein ML. Age-related changes in trabecular architecture differ in female and male C57BL/6J mice. J Bone Miner Res, 2007; 22(8):1197-1207.

66. Willinghamm MD, Brodt MD, Lee KL, Stephens AL, Ye J, Silva MJ. Age-related changes in bone structure and strength in female and male BALB/c mice. Calcified Tissue Int, 2010; 86(6):470-483.

67. Lambers F, *Functional bone imaging in an in vivo mouse model of bone adaptation, aging and disease*. 2011.

68. Klinck RJ, Campbell GM, Boyd SK. Radiation effects on bone architecture in mice and rats resulting from in vivo micro-computed tomography scanning. Med Eng Phys, 2008; 30(7):888-895.

69. Laperre K, Depypere M, van Gastel N, Torrekens S, Moermans K, Bogaerts R, Maes F, Carmeliet G. Development of micro-CT protocols for in vivo follow-up of mouse bone architecture without major radiation side effects. Bone, 2011; 49(4):613-622.

70. Hildebrandt IJ, Su H, Weber WA. Anesthesia and Other Considerations for in Vivo Imaging of Small Animals. ILAR Journal, 2008; 49(1):17-26.

71. Hohlbaum K, Bert B, Dietze S, Palme R, Fink H, Thöne-Reineke C. Severity classification of repeated isoflurane anesthesia in C57BL/6JRj mice—Assessing the degree of distress. PloS One, 2017; 12(6):e0179588.

72. Tremoleda JL, Khalil M, Gompels LL, Wylezinska-Arridge M, Vincent T, Gsell W. Imaging technologies for preclinical models of bone and joint disorders. EJNMMI Res, 2011; 1(1):11-11.

73. Lambers FM, Schulte FA, Kuhn G, Webster DJ, Müller R. Mouse tail vertebrae adapt to cyclic mechanical loading by increasing bone formation rate and decreasing bone

771 resorption rate as shown by time-lapsed in vivo imaging of dynamic bone morphometry.
772 Bone, 2011; 49(6):1340-1350.
773 74. Dai Y, Kiselak T, Clark J, Clore E, Zheng K, Cheng A, Kujoth GC, Prolla TA, Maratos-
774 Flier E, Simon DK. Behavioral and metabolic characterization of heterozygous and
775 homozygous POLG mutator mice. Mitochondrion, 2013; 13(4):282-291.
776 75. Yorke A, Kane AE, Friesen CLH, Howlett SE, O'Blenes S. Development of a Rat
777 Clinical Frailty Index. J Gerontol A Biol Med Sci, 2017; 72(7):897-+.
778 76. Tseng H-C, Lee C-Y, Weng W-L, Shiah IM. Solubilities of amino acids in water at
779 various pH values under 298.15K. Fluid Phase Equilibria, 2009; 285(1):90-95.
780 77. D'Hulst G, Jamart C, Van Thienen R, Hespel P, Francaux M, Deldicque L. Effect of
781 acute environmental hypoxia on protein metabolism in human skeletal muscle. Acta
782 Physiol (Oxf), 2013; 208(3):251-264.
783 78. Rüegsegger P, Koller B, Müller R. A microtomographic system for the nondestructive
784 evaluation of bone architecture. Calcified Tissue Int, 1996; 58(1):24-29.
785 79. Gorski T, Mathes S, Krutzfeldt J. Uncoupling protein 1 expression in adipocytes derived
786 from skeletal muscle fibro/adipogenic progenitors is under genetic and hormonal
787 control. J Cachexia Sarcopenia Muscle, 2018; 9(2):384-399.
788 80. Mayeuf-Louchart A, Hardy D, Thorel Q, Roux P, Gueniot L, Briand D, Mazeraud A,
789 Bougle A, Shorte SL, Staels B, Chretien F, Duez H, Danckaert A. MuscleJ: a high-
790 content analysis method to study skeletal muscle with a new Fiji tool. Skelet Muscle,
791 2018; 8(1):25.

792 **Acknowledgements**

793 We acknowledge Susanne Friedrich for the force-grip assessments. **Funding:** This manuscript
794 is based upon work supported by the Swiss National Science Foundation (SNF IZCNZ0-

174586), the European Cooperation in Science and Technology (COST Action BM1402: MouseAGE) and the European Research Counsil (ERC Advanced MechAGE ERC-2016-ADG-741883). **Author contributions:** ACS and GDH designed the experiments, collected the data and wrote the manuscript, GAK designed the experiments, collected the data and reviewed the manuscript, ME collected the data and reviewed the manuscript, ESW provided support establishing methods and reviewed the manuscript, RM and KDB designed the experiments and wrote the manuscript. **Competing Interests**: All authors declare that they have no conflicts of interest.

## Figures

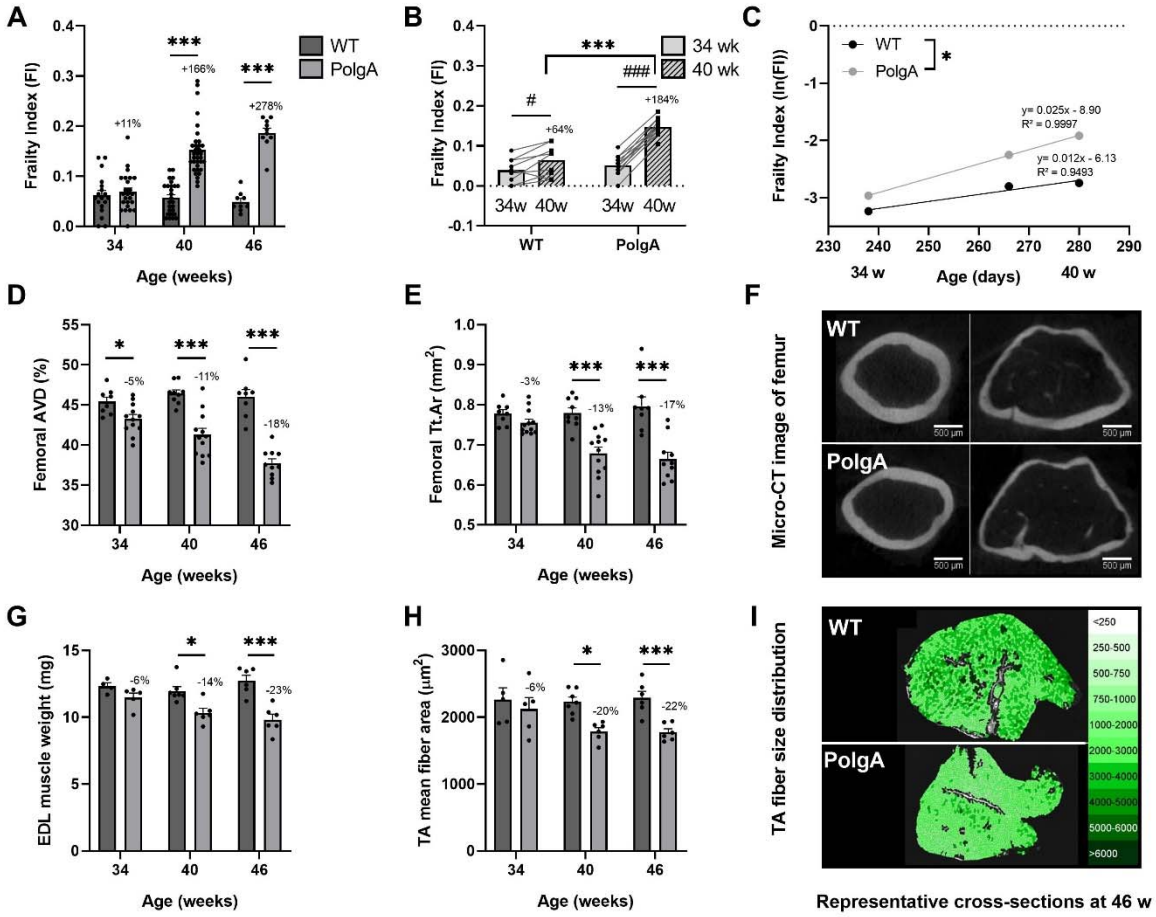


**Fig. 1.** Comparison of the frailty and musculoskeletal phenotypes at different ages. (**A**) Frailty Index (FI) assessed in PolgA and WT at 34, 40 and 46 weeks (n=9-35/group). (**B**) Longitudinal monitoring of FI in individual mice (n=9-12/group) at 34 (light bars) and 40 weeks (striped bars). (**C**) The natural logarithm FI was plotted as a function of age. The slope of the regression lines through these data, which represent the rate of deficit accumulation, was higher in PolgA mice. (**D-I**) PolgA mice displayed lower bone and muscle mass and cross-sectional area compared to WT. (**D**) Apparent volume density (AVD) and (**E**) cross-sectional area (Tt.Ar) of the femoral bone (n=8-12/group). (**G**) Muscle weight and (**H**) fiber area (n=5-7/group). Representative cross-sections of (**C**) femoral bone and (**F**) m. tibialis anterior (TA) muscle of

814 PolgA and WT mice at 46 weeks. (Data represent mean±SEM; * $p<0.05$; ***$p<0.0001$ WT
815 (dark bars) vs PolgA (light bars) determined by student's t-test; for (**B**), ***$p<0.0001$ WT vs
816 PolgA and #$p<0.05$, ###$p<0.0001$ over time determined by two-way ANOVA).
817

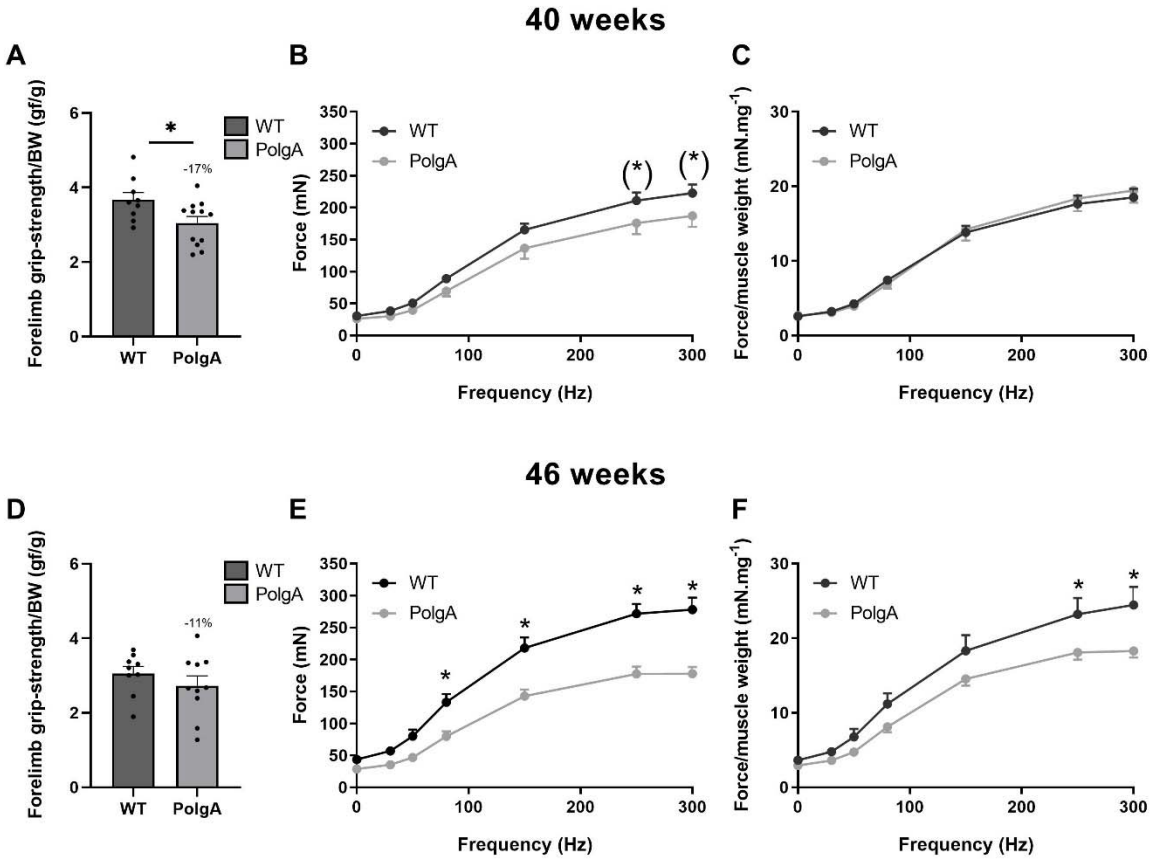


818

819 **Fig. 2.** Muscle phenotyping at 40 (upper row, **A**-**C**) and 46 weeks (lower row, **D**-**F**). (**A**,**D**)
820 Forelimb Grip-Strength (n=9-12/group). (**B**,**E**) Force Frequency at 1, 30, 50, 80, 150, 250, 300
821 Hz. (**C**,**F**) Force frequency relative to EDL muscle weight (n=6-8/group). (Data represent
822 mean±SEM; (*)p<0.10, *p<0.05 by student t-tests (**A**-**D**) and two-way ANOVA (**E**-**H**)).

823

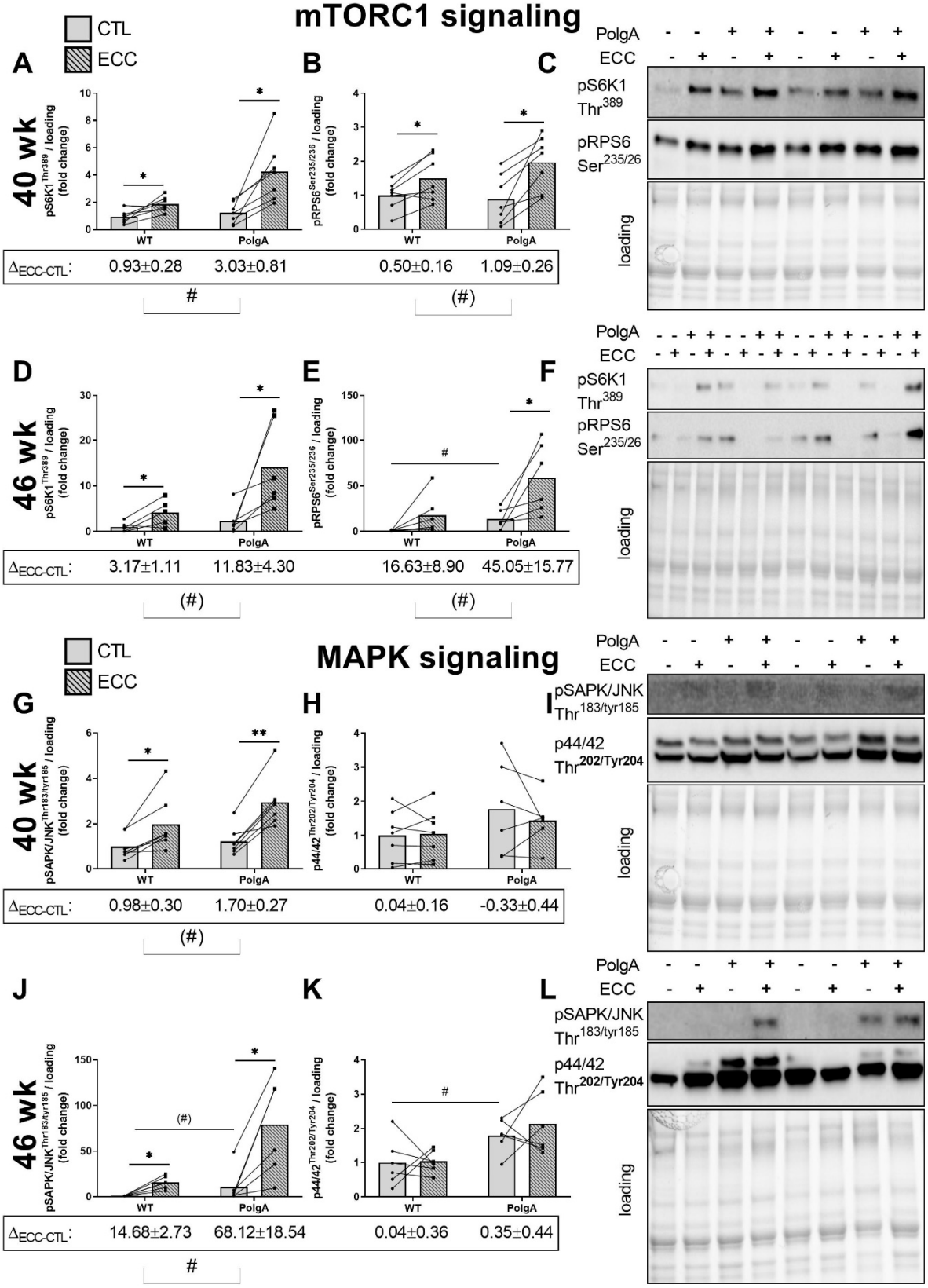


**Fig. 3.** Downstream mTORC1 and MAPK signaling upon eccentric contraction (ECC) in WT and PolgA EDL. Downstream mTORC1 targets pS6K1 and pRPS6 increased upon ECC both

827 at 40 wk (**A**,**B**) and 46 wk (**D**,**E**). (**C**,**F**) representative blots. pSAPK/JNK, but not p44/42
828 MAPK ERK1/2 increased upon ECC both at 40 wk (**G**,**H**) and 46 wk (**J**,**K**). (**I**,**L**) representative
829 blots. (Data represent mean±SEM, n=6-7/group, within genotypes: *$p<0.05$, **$p<0.001$ ECC
830 (squares/striped bars) vs. CTL (circles/light bars) by paired student's t-test, between genotypes:
831 (#)$p<0.10$, #$p<0.05$ by unpaired students t-test ΔECC-CTL and basal values).
832

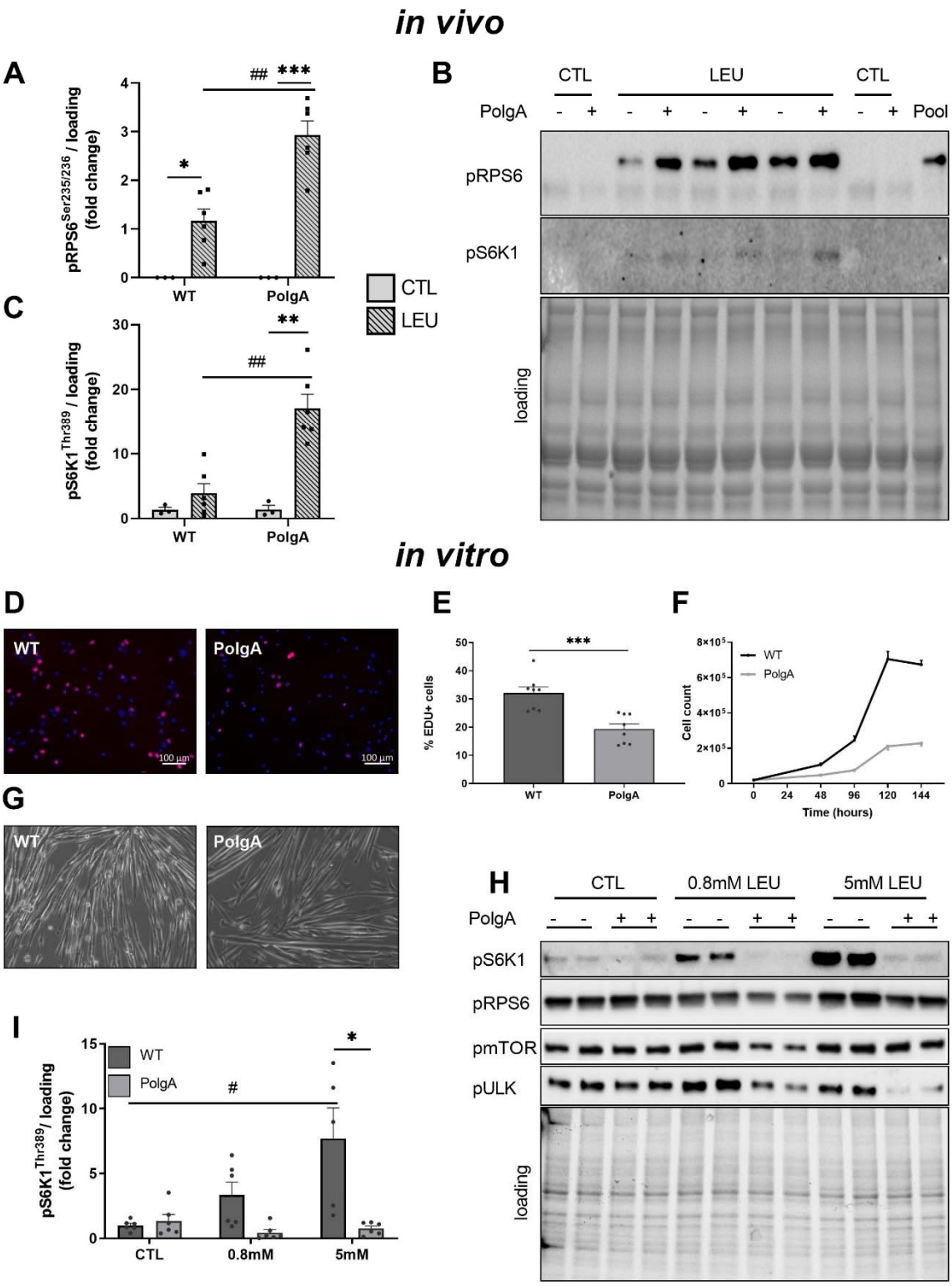


**Fig. 4.** Downstream mTORC1 signaling after leucine administration *in vivo* and *in vitro*. (**A-C**). pRPS6 and pS6K1 signaling 30 min after submaximal dose of leucine gavage *in vivo* in 46-week old WT and PolgA (Data represent mean±SEM, n=3-6/group, within genotypes: *p<0.05,

837 **p<0.001, ***p<0.0001 LEU (squares/striped bars) vs. CTL (circles/light bars), between
838 genotypes: (#)p<0.10, #p<0.05, ##p<0.001 determined by two-way ANOVA). (**C**)
839 Representative blots. (**D**-**I**) Proliferation and downstream mTORC1 signaling in primary
840 myotubes from WT and PolgA muscle. (**D**,**E**) Cell proliferation was analyzed by EdU labelling
841 and (**F**) cell count. (**G**) Brightfield of 2-d differentiated myotubes. (**H**) Representative blots of
842 dose-response leucine experiment in fully differentiated WT and PolgA myoblasts. (**I**)
843 Quantification of pS6K1 from three independent experiments. (Data represent mean±SEM,
844 *p<0.05 WT (dark line/bars) vs PolgA (light line/bars), #p<0.05 over time determined by two-
845 way ANOVA).
846

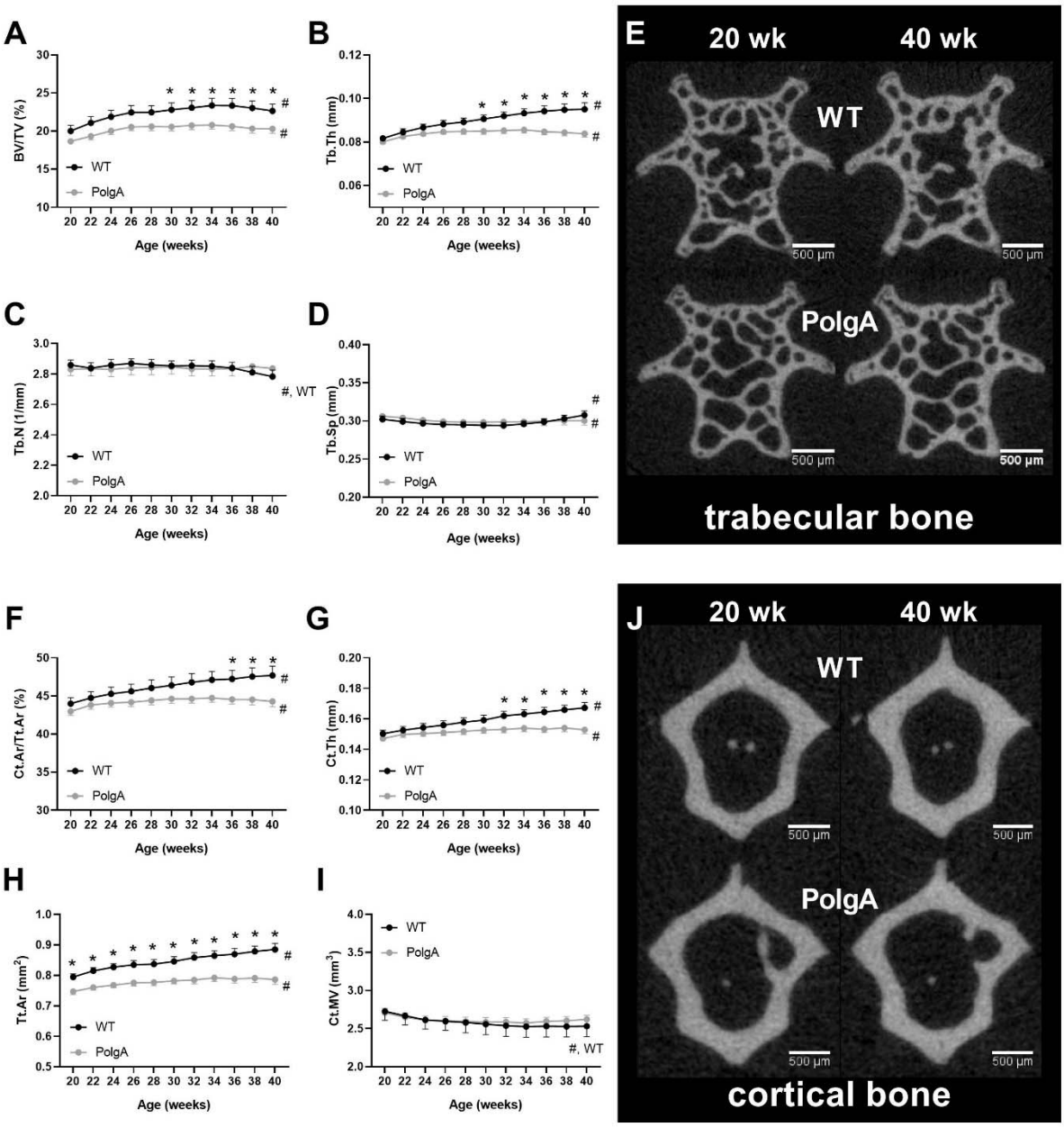


**Fig. 5.** Longitudinal monitoring of trabecular and cortical bone morphometric parameters over 20 weeks: (**A**) bone volume fraction (BV/TV), (**B**) trabecular thickness (Tb.Th), (**C**) trabecular number (Tb.N), (**D**) trabecular separation (Tb.Sp), (**F**) cortical area fraction (Ct.Ar/Tt.Ar), (**G**) cortical thickness (Ct.Th), (**H**) total cross-sectional area (Tt.Ar), and (**I**) cortical marrow volume (Ct.MV). (**E**,**J**) Bone microstructure (cross-sections) of representative (median) WT (top row) and PolgA (bottom row) mice at 20 (left) and 40 (right) weeks of age. In WT mice, thickening of trabeculae and cortex can be observed, while in PolgA mice, little change can be seen

855 between time points. (Data represent mean±SEM; n=9 WT and n=12 PolgA, *p<0.05 WT (dark
856 line) vs PolgA (light line); #p<0.05 over time determined by linear mixed model and Tukey's
857 post hoc).
858

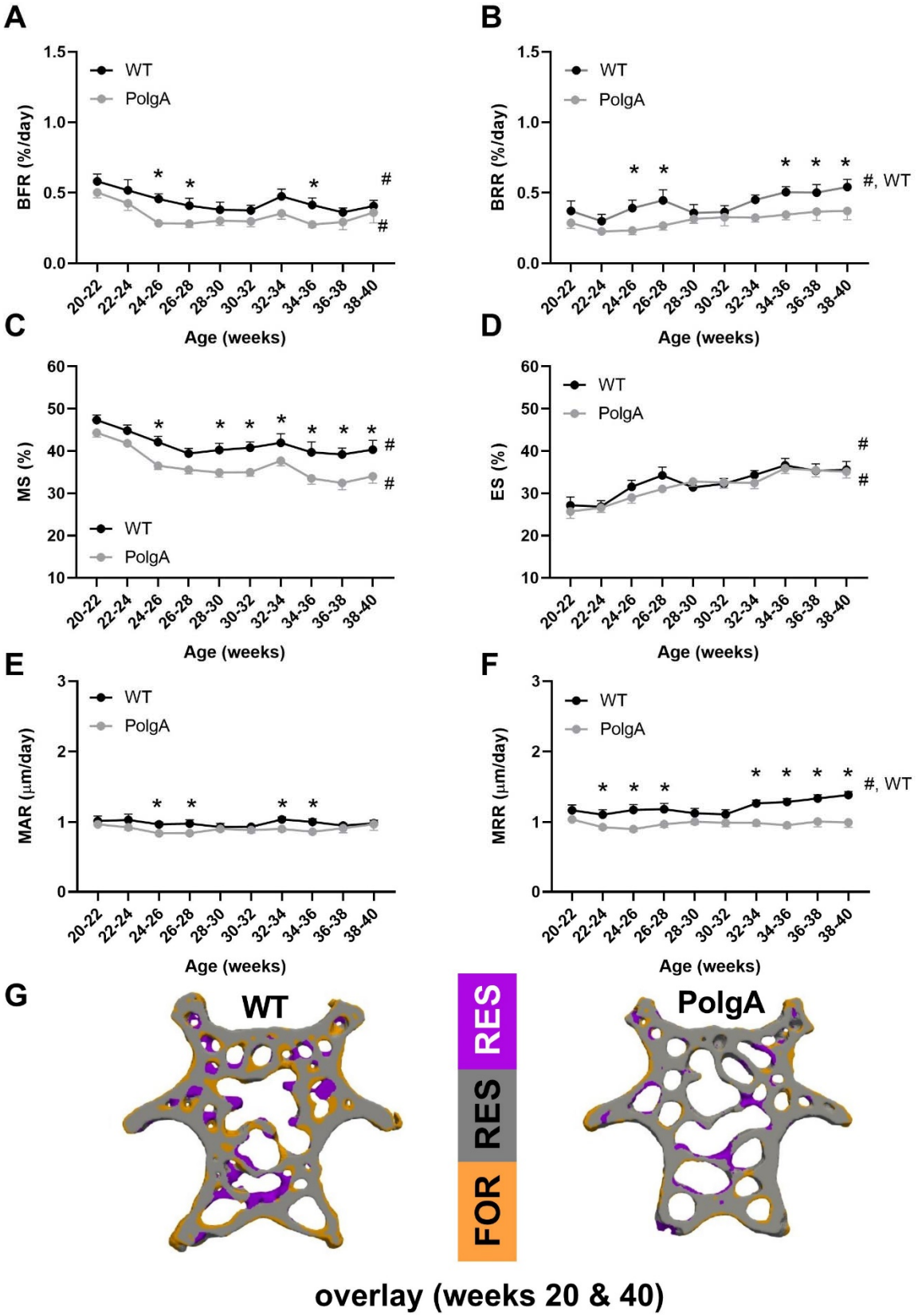


**Fig. 6.** Longitudinal monitoring of dynamic bone morphometry parameters over 20 weeks: (**A**) Bone Formation Rate (BFR), (**B**) Bone Resorption Rate (BRR), (**C**) Mineral Apposition Rate

862 (MAR), (**D**) Mineral Resorption Rate (MRR), (**E**) Mineralizing Surface (MS), and (**F**) Eroding
863 Surface (ES). (Data represent mean±SEM; n=9 WT and n=12 PolgA; *p<0.05 WT (dark line)
864 vs PolgA (light line); #p<0.05 over time determined by linear mixed model and Tukey's post
865 hoc). (**G**) Overlay of thresholded micro-CT images from 20 and 40 weeks showing sites of
866 formation (orange), quiescence (grey) and resorption (blue) in representative WT and PolgA
867 mouse.
868

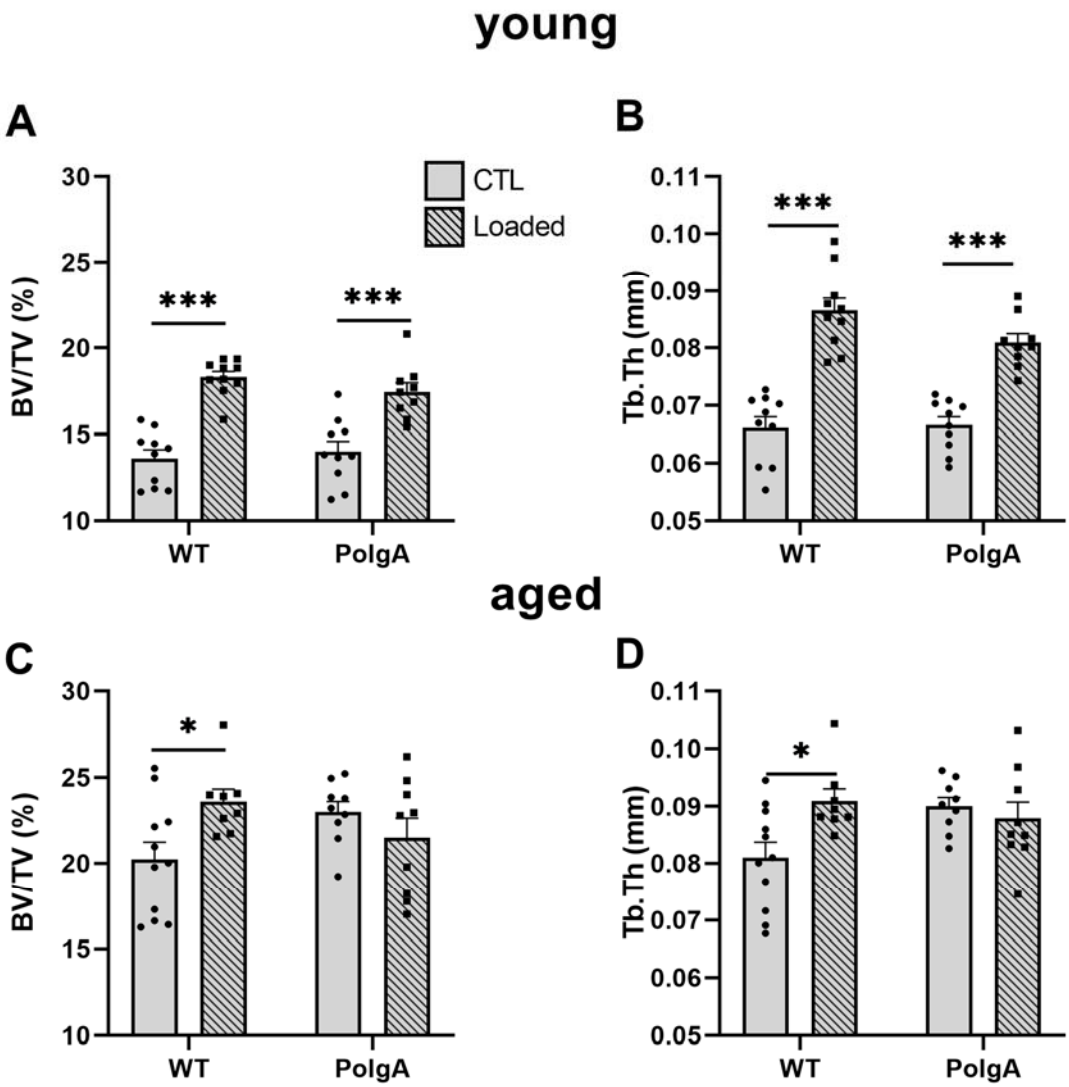


869

870 **Fig. 7.** Effect of cyclic mechanical loading on trabecular bone morphometric parameters in
871 PolgA and WT mice at young (top) and old age (bottom): (**A,C**) bone volume fraction (BV/TV)
872 and (**B,D**) trabecular thickness (Tb.Th) at the end of the loading intervention. (Data represent
873 mean±SEM, n=8-11/group; *p<0.05, ***p<0.0001 CTL (circles/light bars) vs loading
874 (squares/striped bars)).

875

876 **Tables**

**Table 1. Forces eccentric muscle contractions at 40 and 46 weeks**

($^{(*)}$p<0.10, **p<0.001, ***p<0.0001 WT vs PolgA at 40 and 46 weeks, respectively determined by unpaired t-test, corrected for multiple comparisons by Bonferroni)

| | **40 weeks** | | **46 weeks** | |
|---|---|---|---|---|
| Average peak force (mV) | WT | PolgA | WT | PolgA |
| all contractions | 149.9±9.7 | 142.8±15.7 | 141.6±9.6 | 137.3±8.8 |
| 1st set | 193.3±12.4 | 158.8±17.5 | 188.5±6.6 | 164.6±8.6$^{(*)}$ |
| 10th set | 108.8±8.0 | 107.5±11.2 | 98.6±8.2 | 111.8±5.8 |
| Decrease from set 1 to 10 (%) | -43.9±0.9 | -37.5±1.8** | -47.8±3.2 | -32.8±3.8*** |

877

878